Cellulose (2017) 24:977–988
DOI 10.1007/s10570-016-1136-2

ORIGINAL PAPER

Selective adsorption and separation of gadolinium with three-dimensionally interconnected macroporous imprinted chitosan films

Xudong Zheng · Enli Liu · Fusheng Zhang · Jiangdong Dai · Yongsheng Yan · Chunxiang Li

Received: 19 August 2016 / Accepted: 15 November 2016 / Published online: 28 November 2016

Abstract We successfully prepared three-dimensionally interconnected macroporous imprinted chitosan films (3DIM-IFs) by template-assisted assembly. Imprinted chitosan films exhibiting an interconnected macroporous structure are used as adsorbents for efficient and selective adsorption of gadolinium ions (Gd(III)). Saturation adsorption capacity of 3DIM-IFs for Gd(III) is up to 51.36 mg g^{-1} at 298 K, which is significantly higher than adsorption capacities for most reported Gd(III) imprinted adsorbents during recent years. Because of highly selective imprinted sites, imprinted films possess significant selectivity of Gd(III) than other rare earth ions. Moreover, 3DIM-IFs can be easily and rapidly retrieved without the need of additional centrifugation or filtration, greatly facilitating the separation process. Reusability tests demonstrated that the materials can be repeatedly used without significant loss in adsorption capacity, enhancing their potential application for recovery of Gd(III).

Keywords Gadolinium · Adsorption and separation · Chitosan · Imprinted films · 3D Interconnected macroporous

Introduction

Rare earth elements (REEs) have a wide range of applications such as wind turbines, electric vehicles, NiMH batteries, hard disk drives, and fluorescent lamps because of their unique optical, electrical, and magnetic properties (Alonso et al. 2012; Binnemans et al. 2013; Kulaksız and Bau 2013). Especially, gadolinium (Gd) was considered one of most critical metals with the highest supply risk by the European Commission due to its unique characteristics in magnetism and optics (Moss et al. 2013). With ever-increasing demand for high-purity Gd or its compounds, separation and purification of Gd have received considerable attention. However, separation of individual REEs is one of the most difficult tasks because of similar physical–chemical properties derived from their similar ionic radii (Uda et al. 2000).

Liquid–liquid extraction (LLE) is widely used for industrial separation of Gd, which can provide acceptable enrichment needed by multi-step extraction. However, the LLE technique produces significant amounts of undesired effluent. Liquid–solid extraction (LSE) is a greener separation method compared with LLE. Because of its simplicity and high efficiency,

Electronic supplementary material The online version of this article (doi:10.1007/s10570-016-1136-2) contains supplementary material, which is available to authorized users.

X. Zheng · E. Liu · F. Zhang · J. Dai · Y. Yan (✉) · C. Li (✉)
School of Chemistry & Chemical Engineering, Jiangsu University, Zhenjiang 212013, People's Republic of China
e-mail: yanys1@outlook.com

C. Li
e-mail: lcx@mail.ujs.edu.cn

LSE has been considered one of the most promising methods for separation and purification (Sun et al. 2013). Our research group has also successfully synthesized MAH modified mesoporous silica materials with respect to gadolinium adsorption (Zheng et al. 2015). However, adsorbents are usually limited by a lack of adsorption selectivity or adsorption capacity. Thus, extensive efforts have been devoted to the development of the adsorption selectivity and adsorption capacity of REE separation.

Recently, particular attention has been focused on ionic imprinted polymers (IIPs) for adsorption of REEs (Alizadeh and Amjadi 2013; Gao et al. 2014; Li et al. 2015). IIPs are regarded as cost-effective adsorbents with specific ionic recognition sites, which are complementary to target ions (templates). IIPs can be directly cross-linked by linear polymers and functional groups (e.g., glutaraldehyde or epichlorohydrin), which makes the imprinted processes simpler (Branger et al. 2013). Among various functional polymers, chitosan (CS) is one of most popular materials due to its advantages of low cost, abundant functional groups (-NH_2 and -OH), and ease of cross-linking (Yang et al. 2011). As far as we know, almost all the reported CS-based IIPs are processed into powder-like submicron beads (Fu et al. 2015; He et al. 2014; Kyzas et al. 2015). It is difficult to remove completely the templates from the imprinted CS materials because they are embedded. Limited accessibility to imprinted sites significantly impacts adsorption rate and selectivity. Moreover, it is hard to separate submicron beads from solution, which limits its application in industry. Gao's group reported magnetic imprinted chitosan/carbon nanotube nanocomposite (CS/CNT) via surface deposition-cross-linking, and imprinted CS/CNT nanocomposite can be retrieved by magnetism (Li et al. 2015). It provides a valuable rational guide for design of CS-based nanocomposites. However, magnetic submicrospheres were trapped in or adhered to the imprinted CS/CNT network, which inevitably resulted in loss in magnetic spheres during the adsorption procedure.

Immobilizing imprinted CS on surface of structure-directing agent to form porous materials seems to be a possible solution to overcome the previously-mentioned difficulties. Imprinted CS porous materials can facilitate the diffusion of template ions to imprinted sites. Among different porous materials, macroporous material with a three-dimensionally (3D) interconnected pore structure exhibits high surface area, high volume and shows excellent adsorption performance (Fan et al. 2004; Yao et al. 2011; Yu et al. 2011b). In addition, a good film-forming property of CS makes it favorable to prepare 3D interconnected macroporous CS films because the polymer layer can stick tightly on the surface of the sacrificing spheres (Santos et al. 2008). Therefore, design and synthesis of CS-based imprinted 3D interconnected macroporous films with strong combining capacity of Gd(III) and convenient separation from solution seems to be very meaningful.

In this work, we prepared 3D interconnected macroporous imprinted CS films (3DIM-IFs) for adsorption of Gd(III) from solution. 3D interconnected macroporous structure of 3DIM-IFs were characterized by SEM. Adsorption properties of 3DIM-IFs in aqueous solutions were investigated and compared with 3D interconnected macroporous non-imprinted CS films (3DIM-NIFs) and bulk imprinted CS films (bulk imprinting). Effects of pH and temperature on the adsorption were also studied systematically. In addition, the reusability of 3DIM-IFs renders our imprinted CS films possess recycle stability and economically viable for separation of Gd(III).

Experimental

Preparation of materials

Tetraethoxysilane (TEOS, ≥99.9 %), CS (Deacetyiation > 90 %), ammonia, and glutaraldehyde solution were obtained from Aladdin-Reagent (Shang Hai, China, www.aladdin-reagent.com). HAc, ethanol, and $Gd(NO_3)_3{\cdot}6H_2O$ were purchased from Sinopharm Chemical Reagent Co., Ltd. (Shang Hai, China, www.sinoreagent.com). Double distilled water (DDW) was used for preparing all aqueous solutions and cleaning processes.

Synthesis of monodisperse silica particles

Monodispersed silica spheres were prepared using a modified Stöber method (Stöber et al. 1968). Briefly, 25 mL of DDW, 62 mL of ethanol, and 9 mL of ammonia were added into 250-mL of flask under stirring at room temperature for 1 h. Then 4.5 mL of TEOS was added quickly. The mixture was kept for

4 h under stirring. The silica particles were separated by centrifuge, washed repeatedly with ethanol and water, and dried overnight under vacuum.

Synthesis of 3DIM-IFs, 3DIM-NIFs, and bulk imprinting

First, 0.5 g of $Gd(NO_3)_3{\cdot}6H_2O$ was dissolved in 500 mL of CS solution [0.5 g of CS was dissolved in 500 mL of 2 % (v/v) HAc solution], and the solution was stirred vigorously for 2 h to reach an equilibrium of Gd(III) with CS. 3DIM-IFs were assembled via a centrifugation method (Zhang et al. 2009). Monodispersed silica spheres were added to aforementioned CS solution. The complex was ultrasonicated to form emulsion and centrifuged. After the silica spheres were fully precipitated, the redundant CS solution was carefully removed. Then, CS/silica composites were immersed in 5 % (v/v) glutaraldehyde solution for crosslinking of Gd(III)-CS. Cross-linked composite films were eluted with 10 % (v/v) HAc solution to remove of Gd(III) templates, then films were washed with water. Subsequently, silica spheres were removed by 1 M NaOH solution. 3DIM-IFs were obtained by drying in a vacuum chamber. 3DIM-NIFs were synthesized same with 3DIM-IFs except that no Gd(III) templates were added. To prepare bulk imprinting for comparison: 0.5 g of $Gd(NO_3)_3{\cdot}6H_2O$ was first dissolved in 500 mL of CS solution [0.5 g of CS was dissolved in 500 mL of 2 % (v/v) HAc solution], and the solution was stirred vigorously for 2 h to reach an equilibrium of Gd(III) with CS. Thirty milliliters of the mixture was left to dry at room temperature on a polystyrene Petri dish ($d = 8$ cm). Almost three days slow evaporation, bulk imprinted composites were obtained. Composites were immersed in 5 % (v/v) glutaraldehyde solution for crosslinking of Gd(III)-CS. Cross-linked composite films were eluted with 10 % (v/v) HAc solution to remove of Gd(III). Scheme 1 illustrates the detailed fabrication process of 3DIM-IFs.

Batch adsorption experiments

The effect of solution pH on adsorption was investigated first. 3DIM-IFs, 3DIM-NIFs, and bulk imprinting (10 mg) were immersed into different pH of Gd(III) stock solution (10 mL, 50 mg L^{-1}, 298 K) for adsorption. When adsorption equilibrium was reached, final concentrations of Gd(III) were determined by ICP-OES (ICP spectrometer, VARIAN America). The adsorption capacity (Q_t) was determined by the Eq. (1):

$$Q_t = \frac{V(C_0 - C_e)}{W} \quad (1)$$

where C_0 (mg L^{-1}) and C_e (mg L^{-1}) are the initial and equilibrium Gd(III) concentrations in solution, respectively.

Kinetic experiments were conducted at 298 K by varying contact time 5–720 min. 3DIM-IFs, 3DIM-NIFs, and bulk imprinting (10 mg) were immersed to the Gd(III) stock solution (10 mL, 50 mg L^{-1}, pH 7). Equilibrium isotherm experiments were carried out at three different temperatures (298, 308, and 318 K). 3DIM-IFs, 3DIM-NIFs, and bulk imprinting (10 mg) were immersed into a range of initial concentrations of the Gd(III) stock solutions (10 mL, pH 7.0,) to reach equilibrium.

Selectivity recognition properties of 3DIM-IFs for Gd(III) were evaluated by mixed competitive system. Mixed solutions of Gd(III), Dy(III), Tb(III), Pr(III), and Nd(III) were prepared from the standards solutions (pH 7.0, 50 mg L^{-1} for each cations, 298 K). Ten milligrams of 3DIM-IFs and 3DIM-NIFs were added into 10 mL of mixed solutions. Residual cation concentrations of each ion were analyzed by ICP-OES.

Reusability experiments

After the adsorption tests, 3DIM-IFs and 3DIM-NIFs were fetched out of the solution. The films were rinsed with 100 mL of double distilled water. Then materials were regenerated using 10 % (v/v) HAc, then reconditioned 3DIM-IFs and 3DIM-NIFs were used in reusability experiments.

Result and discussion

Characterization of films

The physical–chemical characterization of adsorbent is crucial to prove that it is well developed. Thus, different characterizations have been used to examine

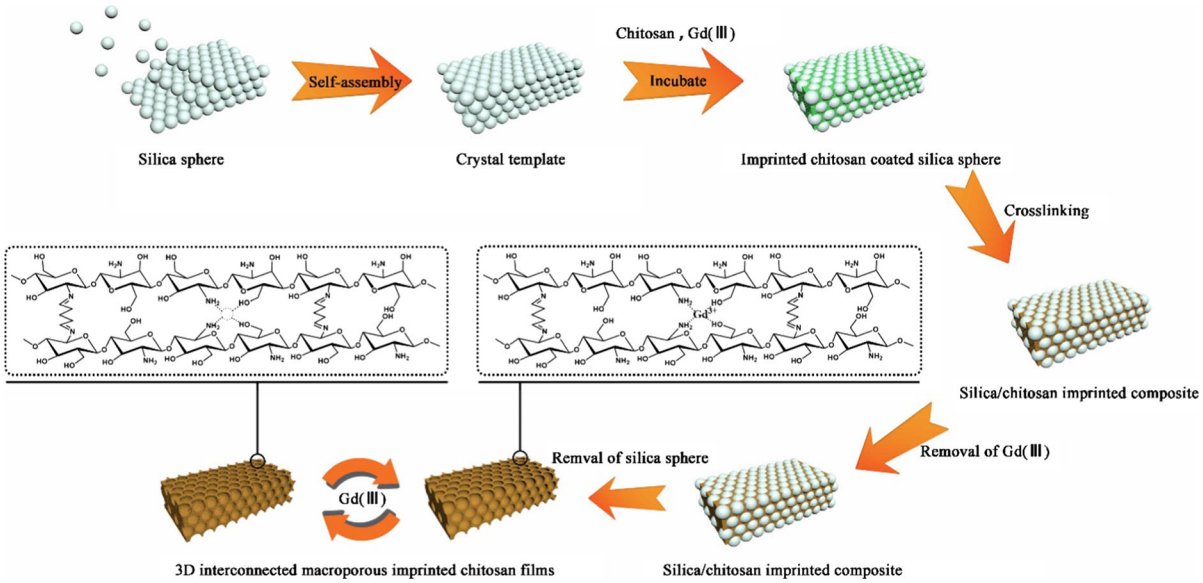

Scheme 1 Schematic of the 3DIM-IFs and adsorption mechanism of Gd(III)

and validate the morphologies and compositions of our imprinted CS film materials.

Structural and surface characterization

The morphological characterization of the three samples (3DIM-IFs, 3DIM-NIFs, and bulk imprinting) were confirmed by scanning electron microscopy (SEM, JEOL, JSM-7001F). Figure 1a reveals the morphology of 3DIM-NIFs that displays a 3D interconnected structure with spherical voids. It is also observed the similar structure in 3DIM-IFs (Fig. 1b). Quasi-spherical cavities of 3DIM-IFs and 3DIM-NIFs is around 200 nm in diameter, which is consistent with the diameter of silica sphere (see Fig. S1a in the Supporting Information). The surface morphology of the bulk imprinted films appears very smooth compared with 3DIM-IFs and 3DIM-NIFs (Fig. S1b). In the SEM images, interconnected macroporous of 3DIM-IFs and 3DIM-NIFs are not ordered. This may be due to polymer shrinkage and deformation after removal of silica sphere.

Nitrogen adsorption studies were employed to characterize 3DIM-IFs, 3DIM-NIFs, and bulk imprinting by a Micromeritics TriStar II 3020 analyzer (Micromeritics Instrument Corporation, USA). All materials were outgassed for 12 h at 80 °C prior to N_2 adsorption analysis, which were carried out at −196 °C. The N_2 adsorption–desorption isotherms for 3DIM-IFs and 3DIM-NIFs are presented in Fig. 2. The N_2 adsorption–desorption isotherm of bulk imprinted films is very low, so we didn't add it in

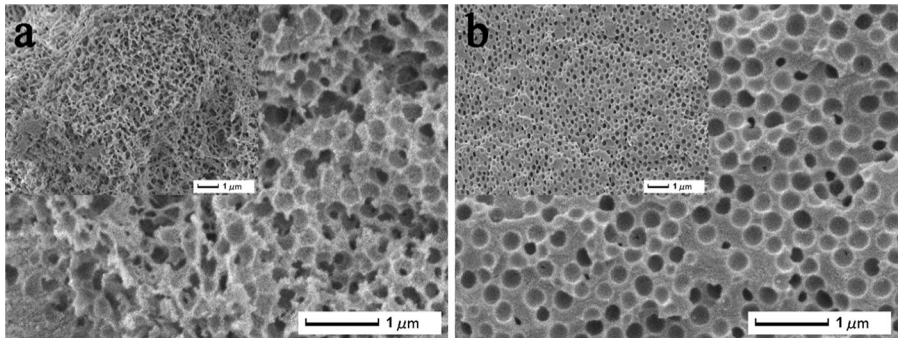

Fig. 1 Representative SEM images of 3DIM-NIFs (**a**) and 3DIM-IFs (**b**) under different magnifications

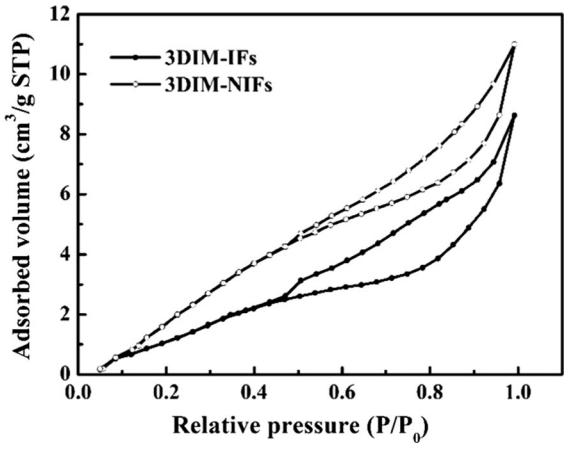

Fig. 2 N_2 adsorption–desorption isotherms for 3DIM-IFs and 3DIM-NIFs

the Fig. 3 DIM-IFs and 3DIM-NIFs exhibit typical type IV isotherms with a distinctive H1 hysteresis loop. Table 1 summarizes the corresponding value of the Brunauer–Emmet–Teller surface areas (S_{BET}) of 3DIM-IFs and 3DIM-NIFs samples; from the table, 3DIM-IFs and 3DIM-NIFs possess the BET surface area of about 14.08 and 19.71 $m^2\ g^{-1}$, respectively. Pore size distributions were only detected between 0.8 and 150 nm, so we did not add the pore size distributions cures in the figure.

The FT-IR spectra (Nicolet NEXUS-470 FT-IR apparatus, USA) of 3DIM-IFs, 3DIM-NIFs, and bulk imprinting were shown in Fig. S2. From the FT-IR results, there are no significant differences with spectra of three materials. By contrast, all the samples

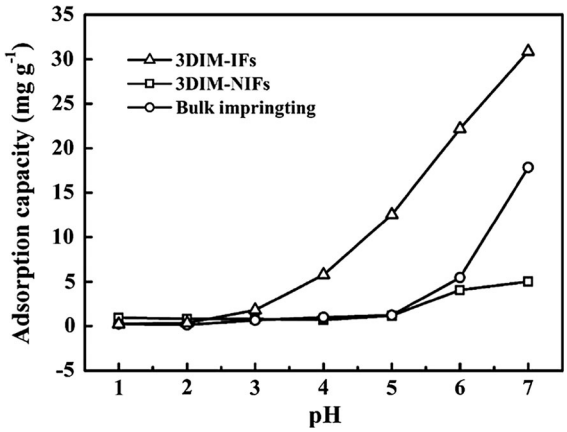

Fig. 3 The effect of pH on the adsorption capacity of 3DIM-IFs, 3DIM-NIFs, and bulk imprinted films (50 mg L^{-1}; 298 K)

Table 1 Brunauer–Emmet–Teller surface areas (S_{BET}) obtained by N_2 adsorption–desorption measurements for 3DIM-IFs and 3DIM-NIFs

Materials	S_{BET} ($m^2\ g^{-1}$)
3DIM-IFs	14.08
3DIM-NIFs	19.71

show distinctive adsorption peaks of chitosan. The broad bands at about 3460 cm^{-1} correspond to the stretching vibration of -NH_2 and -OH. The adsorption bands at about 2930 and 2868 cm^{-1} are assigned to the stretching vibration of -CH, -CH_2, and -CH_3. The adsorption bands at 1604 and 1653 cm^{-1} are assigned to the bending vibration of -NH in -NH_2 and the stretching vibration of C=O in *N*-acetyl groups, respectively. The bands at 1083 cm^{-1} correspond to the stretching vibration of the C–O–C bridge (Wang et al. 2013). The amounts of carbon, hydrogen and nitrogen for all adsorbents were obtained by CHN elemental analysis (Table 2). For all the 3DIM-IFs, 3DIM-NIFs, and bulk imprinting, the contents in these elements are similar.

Adsorption studies

The effect of pH on the adsorption

The solution pH has a significant influence on the adsorption of Gd(III) because it may affect the chemistry of metal ions and the surface properties of the films, which, in turn, influence the affinity of imprinted films for Gd(III). Thus, the effect of pH on 3DIM-IFs, 3DIM-NIFs, and bulk imprinting was investigated by the same experimental procedure. Gd(III) may form insoluble precipitate of $Gd(OH)_3$ in basic solutions. Thus, pH values studied in this work were performed over the range from 1.0 to 7.0. According to the results shown in Fig. 3, it is obvious that the adsorption capacity of Gd(III) progressively

Table 2 Elemental composition of the materials from elemental analysis

Materials	N (%)	C (%)	H (%)
3DIM-IFs	4.032	47.927	7.366
Bulk imprinting	3.701	48.748	7.442
3DIM-NIFs	4.151	45.555	7.013

increases with increasing pH. When the pH increases, the protonation of the CS amino groups decreases, so the adsorption capacity of Gd(III) is enhanced. The adsorption capacity of 3DIM-IFs is significantly higher than 3DIM-NIFs and bulk imprinting. Since the Gd(III) adsorption took place via coordination interactions between Gd(III) ions and amino groups of CS. 3DIM-IFs provided large numbers of adsorption imprinted sites compared with 3DIM-NIFs and bulk imprinting. Fig. S3 reports pH variation with Gd(III) adsorption. Within the pH range of 1.0–4.0, the value of equilibrium pH is close to the initial pH, while in the range of initial pH 4.0–7.0, the final pH tends to decrease by 1 or 2 pH units. This may be attributed to the effect of amine functions from chitosan: with a pK close to 6.3–6.7, amine groups of chitosan bind Gd(III). Since the adsorption of Gd(III) took place on imprinted sites between Gd(III) and amino groups of CS. Under acidic condition, the protonation of amino groups could reduce their binding abilities of chelating with Gd(III). Hence, pH 7.0 is chosen as the initial pH value of solution for the follow-up experiments.

Adsorption kinetics

The kinetic cures of 3DIM-IFs, 3DIM-NIFs, and bulk imprinting shown in Fig. 4 were fitted by pseudo-first-order kinetic model (PFOKM) and pseudo-second-order kinetic model (PSOKM). The corresponding parameters of three films are compiled in Table 3. The adsorption amount of Gd(III) at time t was calculated by the Eq. 2:

$$Q_t = \frac{V(C_0 - C_t)}{W} \tag{2}$$

where Q_t (mg g^{-1}) stands for the adsorption amount of Gd(III) absorbed, C_0 (mg L^{-1}) and C_t (mg L^{-1}) represent the initial and terminate concentrations of Nd(III) after time t, respectively. V and W are the solution volume (L) and mass (g) of adsorbent used in the adsorption experiments, respectively. PFOKM and PSOKM were employed to examine the kinetics data of 3DIM-IFs, 3DIM-NIFs, and bulk imprinting. PFOKM and PSOKM are reported in Eqs. (3) and (4), respectively:

$$Q_t = Q_e - Q_e e^{-k_1 t} \tag{3}$$

$$Q_t = \frac{k_2 Q_e^2 t}{1 + k_2 Q_e t} \tag{4}$$

where Q_t (mg g^{-1}) and Q_e (mg g^{-1}) are the adsorption amounts at time t (min), and at equilibrium, respectively. k_1 (L min^{-1}) and k_2 (g mg^{-1} min^{-1}) are the rate constants of the PFOKM and PSOKM, respectively. The initial adsorption rate h (mg g^{-1} min^{-1}) and half equilibrium time $t_{1/2}$ (min) of the PSOKM also were calculated by the Eqs. 5 and 6 (also see Table 3):[21]

$$h = k_2 Q_e^2 \tag{5}$$

$$t_{1/2} = \frac{1}{k_2 Q_e} \tag{6}$$

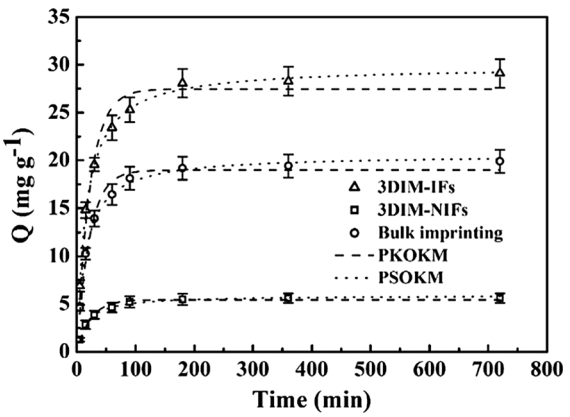

Fig. 4 Kinetic data and modelling for the adsorption of Gd(III) on 3DIM-IFs, 3DIM-NIFs, and bulk imprinted films. *Error bar* represents the standard deviation of the kinetic data (50 mg L^{-1}; 298 K; pH 7)

Figure 4 shows the kinetic curves of films increase rapidly in the first 50 min, then the curves increase gently and finally reaching equilibrium within 2–3 h. This phenomenon may because the adsorption on the exterior surface fast reaches saturation, and then Gd(III) ions take a relatively longer time to diffuse into the pores of films to achieve equilibrium. Nonlinear fittings of adsorption kinetics data with PFOKM and PSOKM for adsorptions are also shown in Fig. 4. The calculated kinetic parameters and the corresponding correlation coefficients (R^2) are compiled in Table 3. It reveals that PSOKM fits the adsorption kinetics well for all the film materials, with correlation coefficients of 0.998, 0.996, and 0.994, respectively. The adsorption capacity of 3DIM-IFs

Table 3 Kinetic constants for the pseudo-first-order and pseudo-second-order models

Materials	$Q_{e,exp}$ (mg g^{-1})	Pseudo-first-order kinetic model				Pseudo-second-order kinetic model			
		$Q_{e,c}$ (mg g^{-1})	k_1 (L min^{-1})	R^2	$Q_{e,c}$ (mg g^{-1})	$k_2 \times 10^{-2}$ (g $mg^{-1}min^{-1}$)	h (mg $g^{-1}min^{-1}$)	$t_{1/2}$ (min)	R^2
3DIM-IFs	29.10	27.45	0.0445	0.957	29.84	0.212	1.891	15.78	0.998
Bulk imprinting	19.89	18.97	0.0464	0.975	20.57	0.323	1.368	15.04	0.996
3DIM-NIFs	5.61	5.44	0.0433	0.976	5.90	1.056	0.367	16.05	0.994

calculated by PSOKM agrees well with the results obtained experimentally. This means the adsorption rate is proportional to the square of the number of imprinted sites, which corresponds to the term $(q_e - q_t)^2$ in PSOKM.(Addo Ntim and Mitra 2011) All the results indicate the chemical process is likely to be the rate-limiting step of the adsorption mechanism. Moreover, the h value for 3DIM-IFs, 3DIM-NIFs, and bulk imprinting were found to followed the order 3DIM-IFs > 3DIM-NIFs > bulk imprinting, indicating that lots of imprinted sites improve the kinetic properties of the films.

Adsorption isotherms

Adsorption isotherm data were conducted by Langmuir and Freundlich isotherm models to find the suitable model for accurately depicting the adsorption processes (Fig. 5). Adsorption isotherms for 3DIM-IFs, 3DIM-NIFs, and bulk imprinting at three different temperatures (298, 308, and 318 K) are shown in Fig. S4. The equations of the Langmuir and Freundlich isotherm are expressed as follows (Mou et al. 2012; Yang et al. 2014):

$$Q_e = \frac{K_L Q_m C_e}{1 + K_L C_e} \tag{7}$$

$$Q_e = K_F C_e^{1/n} \tag{8}$$

where Q_m (mg g^{-1}) represents the maximum adsorption capacity of materials. K_L (L g^{-1}) is Langmuir affinity constant, while K_F (mg g^{-1}) is the Freundlich adsorption capacity direction constant, and $1/n$ is the heterogeneity factor.

Figure 5 shows that the adsorption capacity of 3DIM-IFs is higher than that of 3DIM-NIFs and bulk imprinting under the same condition, which suggests a preference adsorption of 3DIM-IFs for Gd(III). This

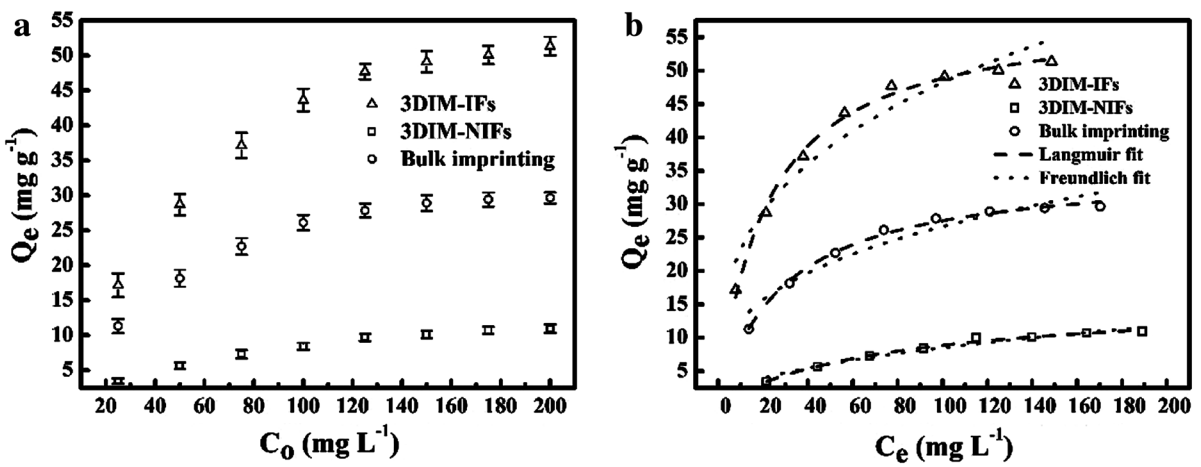

Fig. 5 Equilibrium data (**a**) and modelling (**b**) for the adsorption of Gd(III) on 3DIM-IFs, 3DIM-NIFs, and bulk imprinted films. *Error bar* represents the standard deviation of the kinetic data (298 K; pH 7.0)

may contribute to 3DIM-IFs providing specific imprinted sites for Gd(III) adsorption. The imprinted matrix offers an excellent spatial structure for the coordination of Gd(III) with the two hydroxyl oxygen atoms and two ammonia nitrogens of the chitosan, thus favoring the chelation of Gd(III) ions, resulted in size selectivity towards Gd(III) of a certain radius in acidic solution. Imprinted sites not only can improve the selectivity but also can enhance the mass transfer rate and adsorption capacity for template ions. On the contrary, due to no imprinted sites on the 3DIM-NIFs, the selectivity and adsorption capacity of 3DIM-NIFs are lower than 3DIM-IFs, obviously. The Langmuir isotherm model gives a better fit to the experimental adsorption data with correlation coefficient ($R^2 > 0.94$, Table 4). The Langmuir model is based on the assumption that adsorption sites are identical and energetically equivalent and that adsorption process occurs as a monolayer coverage resulting in finite ionic adsorption. From the experimental data of three films, the adsorption capacities increase until saturation with an increase in Gd(III) content. The experimental saturation adsorption capacities of 3DIM-IFs, 3DIM-NIFs, and bulk imprinting are 51.36, 10.94, and 29.66 mg g^{-1}, which are comparable with the calculated equilibrium capacities (Q_m) by the Langmuir model. The "favorability'' of the adsorption can be evaluated by the separation factor R_L, which is calculated by Eq. (9), where C_m is the maximum initial Gd(III) concentration.

$$R_L = \frac{1}{1 + C_m K_L} \tag{9}$$

The calculated value of R_L indicates that the material is a favorable medium for the adsorption. R_L values of 3DIM-IFs, 3DIM-NIFs, and bulk imprinting were calculated to be 0.0949, 0.2781, and 0.1268, respectively. R_L values of 3DIM-IFs is smaller than that of 3DIM-NIFs, and bulk imprinting, which suggests our designed imprinted film is a more favorable adsorbent for Gd(III).

The effect of temperature on the adsorption

To investigate the thermodynamic parameters, the effect of temperature on the adsorption was carried out at three different temperatures (298, 308, and 318 K) with 100 mg L^{-1} initial concentration of Gd(III). The maximum adsorption capacities of three materials are found to increase slightly with increase in temperature. The adsorption change with temperature is due to the increase in diffusion and decrease in viscosity of solution (Yu et al. 2011a). Thermodynamic equilibrium constant K° was calculated by plotting $\ln(C_s/C_e)$ as a function of C_s (see Fig. S5). C_s is the amount of Gd(III) adsorbed per gram of adsorbents (mmol/g) and C_e is the equilibrium concentration of Gd(III) ions (mmol mL^{-1}). The value of Gibb' s free energy change can be calculated by equation.

$$\Delta G^\circ = -RT\ln K^\circ \tag{10}$$

where R is the universal gas constant (8.3145 J mol^{-1} K^{-1}) and T is the temperature of the solution (K). Table 5 summarizes the calculated values of Gibb's free energy at different temperatures. Standard enthalpy ΔH° and ΔS° can be calculated by the van't Hoff equation:

$$\ln K^\circ = \frac{\Delta S}{R} - \frac{\Delta H}{RT} \tag{11}$$

where T is the absolute temperature (K) of solution. The values of enthalpy change (ΔH°) and entropy change (ΔS°) are calculated by the slope and the intercept of the plot of ln K° versus $1/T$ (Fig. 6), the constants are also compiled in Table 5. Figure 6 shows the effect of increasing temperature on Gd(III) adsorption using 3DIM-IFs, 3DIM-NIFs, and bulk imprinting. Both the positive values of enthalpy change (ΔH°) and the decrease in Gibbs free energy change with the increase of the temperature reveal that the adsorption reaction is endothermic.

Table 4 Adsorption equilibrium constants for Langmuir and Freundlich isotherm equations

Sorbents	Langmuir isotherm equation				Freundlich isotherm equation		
	R^2	K_L (L mg^{-1})	Q_m (mg g^{-1})	R_L	R^2	K_F (mg g^{-1})	$1/n$
3DIM-IFs	0.994	0.0477	59.06	0.0949	0.934	11.136	0.3182
Bulk imprinting	0.995	0.0344	35.50	0.1268	0.926	5.8561	0.3290
3DIM-NIFs	0.997	0.0130	15.65	0.2781	0.971	0.9277	0.4808

Table 5 Thermodynamic parameters for Gd(III) adsorption

Materials	$\Delta H°$ (kJ mol^{-1})	$\Delta S°$ (kJ mol^{-1})	T (K)	$K°$	$\Delta G°$ (kJ mol^{-1})	R^2
3DIM-IFs	42.92	214.52	298	8.49	−5.30	0.996
			308	9.01	−5.63	
			318	9.58	−5.97	
Bulk imprinting	51.22	234.24	298	7.50	−4.99	0.999
			308	8.20	−5.39	
			318	8.80	−5.75	
3DIM-NIFs	40.83	182.83	298	5.49	−4.22	0.995
			308	6.07	−4.62	
			318	6.53	−4.96	

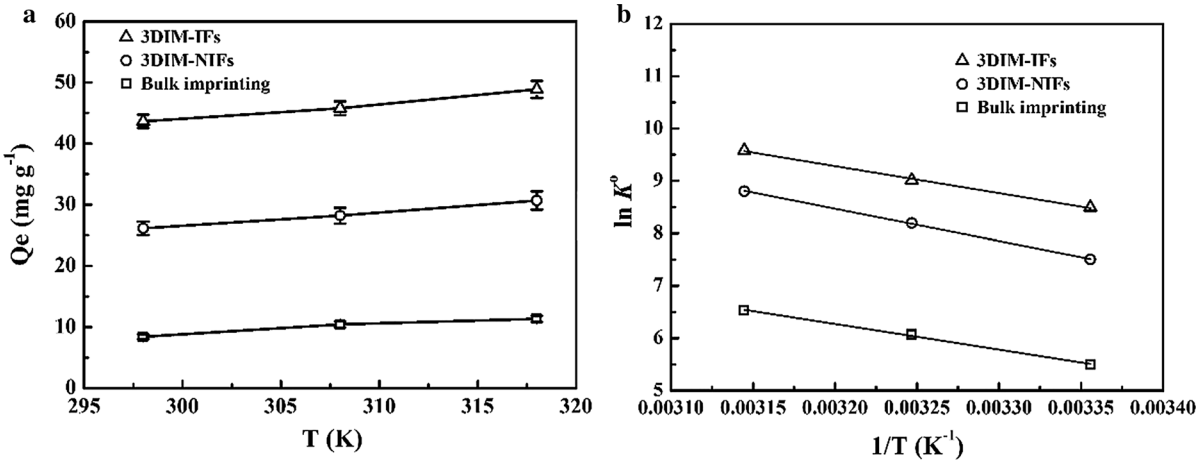

Fig. 6 Thermodynamic properties of Gd(III) on 3DIM-IFs, 3DIM-NIFs, and bulk imprinted films at 298, 308, and 318 K: variation of Q_e with temperature (**a**) and van't Hoff plots of ln $K°$ against $1/T$ (100 mg L^{-1}; pH 7.0) (**b**)

Selective adsorption test

In order to investigate selectivity of the adsorbent, selective tests were performed in a competitive system with Gd(III) and four coexisting anions, including Dy(III), Nd(III), Pr(III), and Tb(III). The adsorption selectivity of 3DIM-IFs with respect to selected ions was evaluated by the distribution coefficients (K_d, mL g^{-1}), selectivity coefficient k, and relative selectivity coefficient k' which were calculated according to Eqs. 12, 13, and 14:

$$k_d = \frac{C_0 - C_f}{C_f} \times \frac{V}{m} \tag{12}$$

$$k = \frac{k_{d1}}{k_{d2}} \tag{13}$$

$$k = \frac{k_{IFs}}{k_{NFs}} \tag{14}$$

where C_0 and C_f stand for the initial and final concentration of each ions, respectively.

Table 6 summarizes the C_f, K_d, k, and k' values of Dy(III), Nd(III), Pr(III), and Tb(III) with respect to Gd(III). In competitive system, Gd(III) adsorption capacity of 3DIM-IFs is found to be much higher than that for other ions. The relative selectivity coefficient (k') is an indicator to reveal an adsorption affinity of selective sites to template ions the k' values of 3DIM-IFs for Gd(III)/Dy(III), Gd(III)/Nd(III), Gd(III)/Pr(III) and Gd(III)/Tb(III) are 2.60-, 4.80-, 3.92-, and 3.37-times greater than those of 3DIM-NIFs, respectively. The great k' value may attribute to specific size of the

Table 6 K_d, k, and k' values of La(III) and Ce(III) with respect to Gd(III) ($C_0 = 50$ mg L^{-1}; pH 7)

Metal ions	3DIM-IFs			3DIM-NIFs			k'
	C_f (mg L^{-1})	K_d (mL g^{-1})	k	C_f (mg L^{-1})	K_d (mL g^{-1})	k	
Gd(III)	28.80	736.38		45.06	109.68		
Dy(III)	42.40	179.20	4.11	46.75	69.56	1.58	2.60
Nd(III)	44.90	113.60	6.48	46.23	81.46	1.35	4.80
Pr(III)	44.19	131.37	5.61	46.45	76.54	1.43	3.92
Tb(III)	41.77	197.01	3.74	45.52	98.44	1.11	3.37

Table 7 Comparison of rare earth elements adsorption performance for different sorbents

Sorbent	Metals	pH	Adsorption capacity (mg g^{-1})	Selectivity	References
Mesoporous silica hybrid materials	Gd(III)	4	76.89	Low	Zheng et al. (2015)
Ionic imprinted resins based on EDTA and DTPA derivatives	Gd(III)	–	24.53	High	Vigneau et al. (2001)
Ion imprinted chitosan/carbon nanotube composite	Gd(III)	7	88	High	Li et al. (2015)
Ion imprinted mesoporous silica	Dy(III)	2	17.45	High	Zheng et al. (2016)
3DIM-IFs	Gd(III)	7	51.36	High	This work

imprinted sites for Gd(III) which is not appropriate for other ions.

The adsorption capacity and selectivity are important benchmarks for the application of adsorbents. Thus, adsorption capacities and selectivity of different adsorbent materials for different REEs, including our previous studies are compared with 3DIM-IFs in Table 7. From the Table, some materials have significantly higher adsorption properties, such as ionic imprinted chitosan/carbon nanotube composite. However, in most cases our 3DIM-IFs have comparable adsorption properties for Gd(III) in pH 7.0. The main advantages of the present materials as excellent adsorbents are the fast kinetics, easy preparation, high adsorption capacity and high selectivity of adsorption and the easy recovery of spent materials at the end of the adsorption process because of membrane properties (Li et al. 2015; Vigneau et al. 2001; Zheng et al. 2016).

Reusability tests

The reusability is a crucial factor of evaluating the value of adsorbents. Thus, five cycling tests were studied to evaluate the regeneration ability of 3DIM-IFs in Fig. 7 (cycling tests of 3DIM-NIFs shown in Fig. S6). From Fig. 7, the adsorption efficiency progressively decreases, but at the fifth cycle the adsorption capacity variation of recycled 3DIM-IFs does not exceed 20 %. The decrease may attribute to the reduction in binding active sites following regeneration and/or an incomplete desorption of the adsorbed Gd(III). The result indicates our prepared film has an excellent stability and can be used as a highly efficient Gd(III) adsorbent.

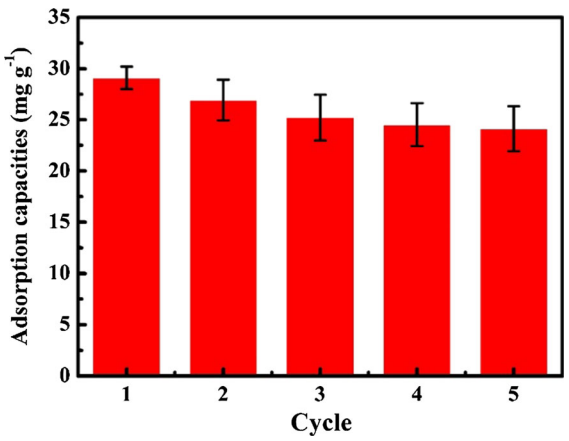

Fig. 7 Regeneration of 3DIM-IFs over five cycles. *Error bars* represent the standard error of the mean for measurements carried out in triplicate (50 mg L^{-1}; 298 K; pH 7.0)

Conclusions

3DIM-IFs were prepared successfully by a template-assisted assembly. The imprinted films were able to adsorb Gd(III) selectively. Compared with traditional bulk imprinted CS films, 3DIM-IFs increased the adsorption amount of Gd(III) due to 3D interconnected macroporous structure. In particular, under optimal pH, 3DIM-IFs exhibit the highest adsorption capacity of 51.36 mg g^{-1} at 298 K. The adsorption kinetics of 3DIM-IFs was found to follow pseudo-second-order type sorption kinetics. The adsorption isotherms of 3DIM-IFs were modelled by the Langmuir isotherm better, which revealed a monolayer adsorption. Because of imprinted sites on 3DIM-IFs, adsorption selectivity of 3DIM-IFs improve significantly. K_d of 3DIM-IFs for Gd(III) is 736.38 mL g^{-1}. Comparing with other adsorbents, cheap sources of chitosan, easy preparation, high adsorption selectivity and adsorption capacity, and rapidly retrieved make our film a good candidate for adsorption of Gd(III) in solution. In addition, reusability tests indicate that our adsorbent has a great potential application for industrial adsorption of Gd(III).

Acknowledgments This work was financially supported by the National Natural Science Foundation of China (No. 21576120, No. 21446015, No. U1507115, and No. U1507118) and Natural Science Foundation of Jiangsu Province (No. BK20140534, No. BK20140580, No. BK20151350, and No. BK20131223).

References

Addo Ntim S, Mitra S (2011) Removal of trace arsenic to meet drinking water standards using iron oxide coated multiwall carbon nanotubes. J Chem Eng Data 56:2077–2083

Alizadeh T, Amjadi S (2013) Synthesis of nano-sized Eu 3+-imprinted polymer and its application for indirect voltammetric determination of europium. Talanta 106:431–439

Alonso E, Sherman AM, Wallington TJ, Everson MP, Field FR, Roth R, Kirchain RE (2012) Evaluating rare earth element availability: a case with revolutionary demand from clean technologies. Environ Sci Technol 46:3406–3414

Binnemans K, Jones PT, Blanpain B, Van Gerven T, Yang Y, Walton A, Buchert M (2013) Recycling of rare earths: a critical review. J Clean Prod 51:1–22

Branger C, Meouche W, Margaillan A (2013) Recent advances on ion-imprinted polymers. React Funct Polym 73:859–875

Fan J, Wang T, Yu C, Tu B, Jiang Z, Zhao D (2004) Ordered, nanostructured tin-based oxides/carbon composite as the negative-electrode material for lithium-ion batteries. Adv Mater 16:1432–1436

Fu J, Chen L, Li J, Zhang Z (2015) Current status and challenges of ion imprinting. J Mater Chem A 3:13598–13627

Gao B, Zhang Y, Xu Y (2014) Study on recognition and separation of rare earth ions at picometre scale by using efficient ion-surface imprinted polymer materials. Hydrometallurgy 150:83–91

He J, Lu Y, Luo G (2014) Ca (II) imprinted chitosan microspheres: an effective and green adsorbent for the removal of Cu (II), Cd (II) and Pb(II) from aqueous solutions. Chem Eng J 244:202–208

Kulaksız S, Bau M (2013) Anthropogenic dissolved and colloid/nanoparticle-bound samarium, lanthanum and gadolinium in the Rhine River and the impending destruction of the natural rare earth element distribution in rivers. Earth Planet Sci Lett 362:43–50

Kyzas GZ, Siafaka PI, Pavlidou EG, Chrissafis KJ, Bikiaris DN (2015) Synthesis and adsorption application of succinyl-grafted chitosan for the simultaneous removal of zinc and cationic dye from binary hazardous mixtures. Chem Eng J 259:438–448

Li K et al (2015) Selective adsorption of Gd3+ on a magnetically retrievable imprinted chitosan/carbon nanotube composite with high capacity. ACS Appl Mater Interfaces 7:21047–21055

Moss R et al (2013) Critical metals in the path towards the decarbonisation of the EU energy sector assessing rare metals as supply-chain bottlenecks in low-carbon energy technologies JRC report EUR 25994

Mou F, Guan J, Ma H, Xu L, Shi W (2012) Magnetic iron oxide chestnutlike hierarchical nanostructures: preparation and their excellent arsenic removal capabilities. ACS Appl Mater Interfaces 4:3987–3993

Santos D, Neto C, Fonseca J, Pereira M (2008) Chitosan macroporous asymmetric membranes—preparation, characterization and transport of drugs. J Membr Sci 325:362–370

Stöber W, Fink A, Bohn E (1968) Controlled growth of monodisperse silica spheres in the micron size range. J Colloid Interface Sci 26:62–69. doi:10.1016/0021-9797(68)90272-5

Sun Y, Shao D, Chen C, Yang S, Wang X (2013) Highly efficient enrichment of radionuclides on graphene oxide-supported polyaniline. Environ Sci Technol 47:9904–9910

Uda T, Jacob KT, Hirasawa M (2000) Technique for enhanced rare earth separation. Science (Washington, DC) 289:2326–2329. doi:10.1126/science.289.5488.2326

Vigneau O, Pinel C, Lemaire M (2001) Ionic imprinted resins based on EDTA and DTPA derivatives for lanthanides (III) separation. Anal Chim Acta 435:75–82

Wang S, Zhai Y-Y, Gao Q, Luo W-J, Xia H, Zhou C-G (2013) Highly efficient removal of acid red 18 from aqueous solution by magnetically retrievable chitosan/carbon nanotube: batch study, isotherms, kinetics, and thermodynamics. J Chem Eng Data 59:39–51

Yang F, Liu H, Qu J, Paul Chen J (2011) Preparation and characterization of chitosan encapsulated Sargassum sp. biosorbent for nickel ions sorption. Bioresour Technol 102:2821–2828. doi:10.1016/j.biortech.2010.10.038

Yang S, Han C, Wang X, Nagatsu M (2014) Characteristics of cesium ion sorption from aqueous solution on bentonite- and carbon nanotube-based composites. J Hazard Mater 274:46–52

Yao Y et al (2011) Interconnected silicon hollow nanospheres for lithium-ion battery anodes with long cycle life. Nano Lett 11:2949–2954

Yu X-Y et al (2011a) Adsorption of lead (II) on O_2-plasma-oxidized multiwalled carbon nanotubes: thermodynamics, kinetics, and desorption. ACS Appl Mater Interfaces 3:2585–2593

Yu Y, Gu L, Lang X, Zhu C, Fujita T, Chen M, Maier J (2011b) Li storage in 3D nanoporous Au-supported nanocrystalline tin. Adv Mater 23:2443–2447

Zhang J et al (2009) Creation of three-dimensionally ordered macroporous Au/CeO_2 catalysts with controlled pore sizes and their enhanced catalytic performance for formaldehyde oxidation. Appl Catal B 91:11–20. doi:10.1016/j.apcatb.2009.05.001

Zheng X, Wang C, Dai J, Shi W, Yan Y (2015) Design of mesoporous silica hybrid materials as sorbents for the selective recovery of rare earth metals. J Mater Chem A 3:10327–10335. doi:10.1039/c4ta06860b

Zheng X, Liu E, Zhang F, Yan Y, Pan J (2016) Efficient adsorption and separation of dysprosium from NdFeB magnets in acidic system by ion imprinted mesoporous silica sealed in dialysis bag. Green Chem